

# ZC3H12C expression in dendritic cells is necessary to prevent lymphadenopathy of skin-draining lymph nodes

Elise Clayer<sup>1,2,3</sup>, Daniel Frank<sup>1,2</sup>, Holly Anderton<sup>1,2</sup>, Shengbo Zhang<sup>1,2</sup>, Andrew Kueh<sup>1,2</sup>, Valentin Heim<sup>1,2,4</sup>, Stephen L Nutt<sup>1,2</sup> , Michaël Chopin<sup>1,2a</sup> & Philippe Bouillet<sup>1,2</sup>

1 The Walter and Eliza Hall Institute of Medical Research, Parkville, VIC, Australia

2 Department of Medical Biology, The University of Melbourne, Melbourne, VIC, Australia

3 ZAUM – Centre of Allergy and Environment, Helmholtz Centre and Technical University of Munich, Munich, Germany

4 Immatic Biotechnologies GmbH, Munich, Germany

## Keywords

dendritic cells, lymphadenopathy, Regnase-3, RNA-binding protein, tumor necrosis factor

## Correspondence

Michaël Chopin and Philippe Bouillet, The Walter and Eliza Hall Institute of Medical Research, 1G Royal Parade, Parkville, VIC 3052, Australia.

E-mails: chopin@wehi.edu.au (MC); bouillet@wehi.edu.au (PB)

<sup>a</sup>These authors share senior authorship.

Received 5 October 2021;

Revised 23 November 2021 and 14 January 2022;

Accepted 17 January 2022

doi: 10.1111/imcb.12521

*Immunology & Cell Biology* 2022; **100**: 160–173

## INTRODUCTION

Cells of the innate immune system produce a host of proinflammatory cytokines to coordinate the fight against pathogens. Expression of these cytokines needs to be tightly regulated to prevent autoimmune conditions that result from their overexpression.<sup>1,2</sup> The role of RNA-binding proteins (RBPs) in the control of cytokine production and the prevention of autoimmunity is increasingly recognized. RBPs are thought to bind elements contained within their target RNAs and control splicing, translation, stability and degradation of these RNAs post-transcriptionally.

Dysregulation of tumor necrosis factor (TNF) expression has been widely reported as a major cause of several inflammatory diseases such as rheumatoid

## Abstract

The role of RNA-binding proteins of the CCCH-containing family in regulating proinflammatory cytokine production and inflammation is increasingly recognized. We have identified ZC3H12C (Regnase-3) as a potential post-transcriptional regulator of tumor necrosis factor expression and have investigated its role *in vivo* by generating *Zc3h12c*-deficient mice that express green fluorescent protein instead of ZC3H12C. *Zc3h12c*-deficient mice develop hypertrophic lymph nodes. In the immune system, ZC3H12C expression is mostly restricted to the dendritic cell (DC) populations, and we show that DC-restricted ZC3H12C depletion is sufficient to cause lymphadenopathy. ZC3H12C can regulate *Tnf* messenger RNA stability via its RNase activity *in vitro*, and we confirmed the role of *Tnf* in the development of lymphadenopathy. Finally, we found that loss of ZC3H12C did not impact the outcome of skin inflammation in the imiquimod-induced murine model of psoriasis, despite *Zc3h12c* being identified as a risk factor for psoriasis susceptibility in several genome-wide association studies. Our data suggest a role for ZC3H12C in DC-driven skin homeostasis.

arthritis, inflammatory bowel disease or psoriasis.<sup>3–6</sup> The role of the 3' untranslated region (3' UTR) of *Tnf* messenger RNA (mRNA) in the post-transcriptional regulation of TNF expression was discovered three decades ago.<sup>7</sup> Tristetraprolin (aka ZFP36), a CCCH-zinc finger-containing RBP, binds to the AU-rich element (ARE) within *Tnf* 3' UTR and mediates its degradation. Tristetraprolin-deficient mice display an inflammatory phenotype due in part to the overexpression of TNF.<sup>8</sup> Mice in which the ARE has been deleted from *Tnf* 3' UTR develop symptoms reminiscent of rheumatoid arthritis and ankylosing spondylitis as well as inflammatory bowel disease.<sup>9</sup> *Tnf* 3' UTR also contains a constitutive decay element<sup>10</sup> and a new regulatory element that we have identified.<sup>11</sup> We have demonstrated that ARE, constitutive decay element and new regulatory

element cooperate to control the stability of *Tnf* mRNA. Indeed, combined deletion of two of these elements caused very high levels of TNF that resulted in embryonic death *in vivo*.<sup>11,12</sup>

Over the last few years, more than 1500 RBPs have been identified and characterized in the human genome.<sup>13</sup> At least 20 RBPs have been shown to interact with the ARE alone, some promoting the stabilization, others the degradation of ARE-containing transcripts.<sup>14</sup> RBPs are classed into different categories and subcategories depending on their structure. Among other roles, zinc finger proteins (ZFPs) regulate immune homeostasis and the associated maturation and activation of innate immune cells through the control of cytokine production.<sup>15</sup> ZFPs such as ZFP36 also play a role in regulating skin homeostasis, as studies have highlighted the decreased expression of *Zfp36* in psoriatic fibroblasts and the spontaneous development of skin inflammation and exacerbation of symptoms using the imiquimod (IMQ)-induced psoriasis model in keratinocyte-specific ZFP36-deficient mice.<sup>16,17</sup> In a reporter screen aimed at identifying potential new regulators of *Tnf* mRNA stability, we highlighted ZC3H12C as an interesting candidate among the family of CCCH-containing ZFPs.<sup>9,11,12</sup>

ZC3H12C, also known as Regnase-3, belongs to the same subfamily of ZFPs as ZC3H12A (Regnase-1), which is a very well-characterized master RNA regulator in macrophages and T cells.<sup>18</sup> Particularly, ZC3H12A has been described as a negative regulator of inflammatory cytokines, especially IL-6, and targets their transcript 3' UTRs independently of the ARE, ultimately leading to their destabilization.<sup>18,19</sup> Previous studies have identified ZC3H12C as a regulator of macrophage activation.<sup>20,21</sup> Adding to this, a large collaborative project of genome-wide association scans published a list of 15 newly identified genes, including *Zc3h12c*, involved in psoriasis susceptibility in humans, pointing for its potential role in controlling skin homeostasis.<sup>22</sup> In this study, we showed that ZC3H12C protein levels are highest in dendritic cells (DCs) rather than in macrophages, and we strived to unravel the physiological role of this protein in inflammation and skin immunity using *Zc3h12c*-deficient and DC-specific *Zc3h12c*-deficient mouse models.

## RESULTS

### ZC3H12C destabilizes *Tnf* 3' UTR *in vitro* mostly via its RNase domain

To identify RBPs involved in the post-transcriptional regulation of *Tnf*, we screened the entire CCCH-containing family of RBPs using a green fluorescent

protein (GFP) reporter assay and identified ZC3H12C as the second most potent negative regulator of *Tnf* expression in this assay after ZFP36 (Supplementary figure 1, see also Lacey *et al.*<sup>11</sup>). The ZC3H12 subfamily of RBPs contains four members, ZC3H12A, ZC3H12B, ZC3H12C and ZC3H12D. Each member contains both a CCCH type of zinc finger motif (ZFM) and a PiIT N-terminus like RNase domain. The CCCH type of ZFM contains three cysteine residues and one histidine in a unique C(X)<sub>a</sub>C(X)<sub>b</sub>C(X)<sub>c</sub>H arrangement. Mutation of a single cysteine residue to an arginine in ZFP36 ZFM was sufficient to abrogate the RNA-binding activity of the protein.<sup>23</sup> Structural and functional analyses of human ZC3H12A PiIT N-terminus like domain highlighted four aspartic acid (Asp) residues forming a catalytic site stabilizing Mg<sup>2+</sup> binding, thus conferring RNase activity to the protein.<sup>24</sup> Point mutation of any of those aspartic

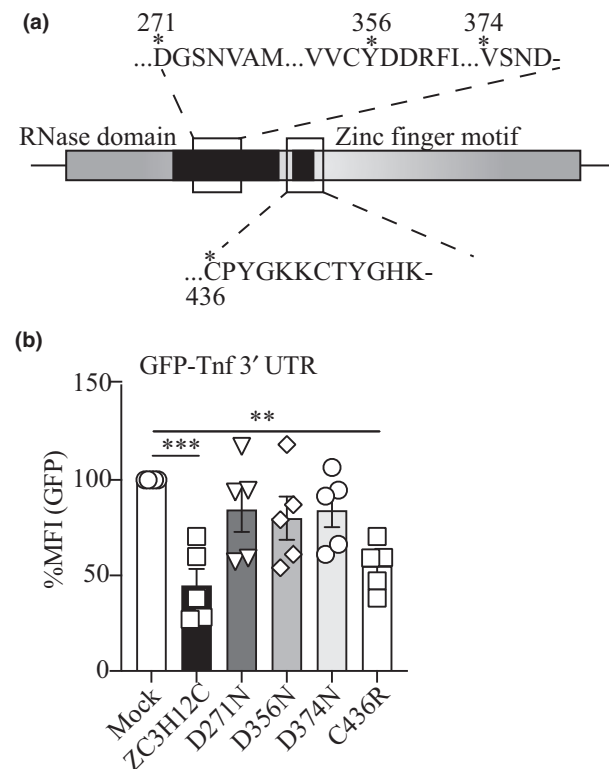


**Figure 1.** Destabilization of the *Tnf* 3' UTR by ZC3H12C. **(a)** Schematic representing the four aspartic residues forming the catalytic site within the RNase domain, and the three cysteines and one histidine residues forming the zinc finger motif. The asterisks represent each mutated residue. **(b)** The destabilizing effect of each of the point mutants of ZC3H12C was assessed using the GFP-*Tnf* 3' UTR reporter assay. Results represent the mean  $\pm$  s.e.m. of three independent experiments. Statistical analysis was performed by two-way ANOVA. \*\* $P < 0.01$ ; \*\*\* $P < 0.001$ . GFP, green fluorescent protein; MFI, mean fluorescent intensity.

residues to asparagine significantly impacted the RNase activity of the protein.<sup>25</sup> To further test the regulatory function of ZC3H12C on *Tnf* 3' UTR, we engineered similar point mutations in the ZFM (C436R) and the RNase (D271N, D356N and D374N) domains (Figure 1a) and tested them in our GFP reporter assay. In our system, all the mutations in the RNase domain almost completely abrogated the destabilizing activity of ZC3H12C on *Tnf* 3' UTR (Figure 1b). By contrast, the mutation C346R in the ZFM only affected the destabilizing effect of ZC3H12C moderately.

### Generation of the *Zc3h12c*-floxed and *Zc3h12c*-GFP alleles

To facilitate the analysis of ZC3H12C function, we generated a *Zc3h12c*-GFP reporter allele in which the GFP complementary DNA (cDNA) sequence (with its stop codon) was added in frame in *Zc3h12c* exon 2. A

polyadenylation signal present in exon 2 terminates the transcript. Therefore, cells with this allele now express GFP in lieu of ZC3H12C under the activity of the *Zc3h12c* promoter (Figure 2a). *Zc3h12c*-GFP<sup>KI/KI</sup> mice no longer express ZC3H12C and can be used to study the expression of ZC3H12C with great sensitivity and in different cell populations by monitoring GFP fluorescence using flow cytometry. We also generated a floxed allele in which loxP sites were inserted on either side of exon 2 (Figure 2a). These mice were first crossed with cre deleter mice to inactivate the gene completely. The genetic modifications in the mice were confirmed using polymerase chain reaction and Sanger sequencing. Complete ablation of *Zc3h12c* in both models led to the same phenotype (see below), and we used *Zc3h12c*-GFP reporter mice for most experiments.

According to the public database *ImmGen*, the highest expression of *Zc3h12c* in the hematopoietic system is in DCs (<http://rstats.immgen.org/Skyline/skyline.html>). To

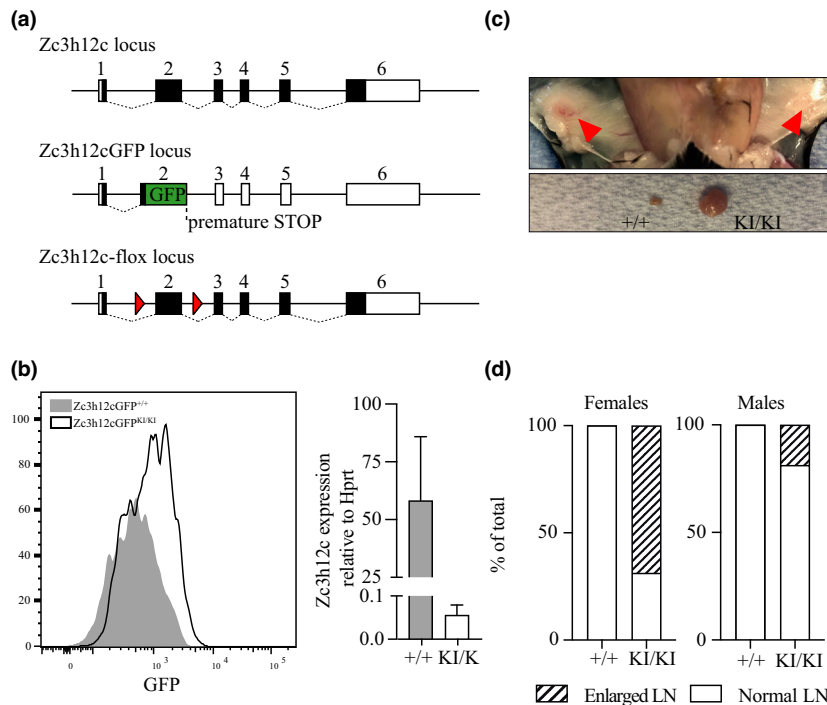


**Figure 2.** Generation and phenotyping of *Zc3h12c*-GFP and *Zc3h12c*-flox mice. **(a)** *Zc3h12c* is located on mouse chromosome 9 and consists of 6 exons (coding sequence is shown in black, noncoding sequences in white). To generate the *Zc3h12c*-GFP mouse strain, the GFP sequence (with its own stop codon) was inserted in-frame within exon 2 of the *Zc3h12c* gene, and a polyadenylation signal (AATAAA) present in exon 2 causes early truncation of the RNA. A *Zc3h12c* flox allele was generated by flanking exon 2 with loxP sites (red arrowheads). **(b)** Bone marrow-derived dendritic cells were cultured for 9 days using Flt3-L and were analyzed by flow cytometry for GFP expression. Representative histogram from three samples. The same cells were used for quantitative PCR analysis to check for *Zc3h12c* messenger RNA with primers located in exons 3 and 4. Results represent the mean  $\pm$  s.e.m. of four independent samples. **(c)** Example of a *Zc3h12c*-GFP<sup>KI/KI</sup> mouse presenting with an enlargement of the right (mouse's side) inguinal lymph node while the left inguinal lymph node remained of average size. The bottom picture shows the size difference between a lymph node from a wild-type mouse and an enlarged lymph node from a *Zc3h12c*-GFP<sup>KI/KI</sup> mouse. **(d)** The proportion of lymphadenopathy (patterned area) observed in females and males in *Zc3h12c*-GFP<sup>+/+</sup> ( $n = 9$ ) and *Zc3h12c*-GFP<sup>KI/KI</sup> ( $n = 17$ ) mice between 3 and 6 months of age. GFP, green fluorescent protein; KI, knock-in; LN, lymph node.

verify the correct insertion of GFP in the *Zc3h12c* locus, we analyzed *Zc3h12c-GFP<sup>KI/KI</sup>* bone marrow-derived DCs (BMDCs) and confirmed that they indeed express GFP (Figure 2b). To confirm the loss of *Zc3h12c*, we also used these BMDCs to analyze *Zc3h12c* expression by quantitative PCR using primers targeting exons 3 and 4 downstream of GFP. As expected, *Zc3h12c-GFP<sup>KI/KI</sup>* BMDCs did not express *Zc3h12c* transcripts (Figure 2b).

A *Zc3h12c*-deficient mouse strain previously reported was shown to develop lymphadenopathy in the skin-draining lymph nodes (sLNs).<sup>21</sup> Our *Zc3h12c-GFP<sup>KI/KI</sup>* mice also developed lymphadenopathy (Figure 2c), confirming that they are indeed *Zc3h12c* deficient. Mice lacking *Zc3h12c*, either heterozygous (*Zc3h12c-GFP<sup>+ / KI</sup>*) or homozygous (*Zc3h12c-GFP<sup>KI / KI</sup>*), were healthy, fertile and their distribution was Mendelian. Lymph node hyperplasia developed in homozygous animals from 3 months of age but did not impact their life span or overall health. As previously observed,<sup>21</sup> lymphadenopathy was limited to sLNs (i.e. brachial, axillary, inguinal and cervical), and we never observed enlargement of mucosal nodes such as mesenteric lymph nodes. While some *Zc3h12c-GFP<sup>KI / KI</sup>* mice showed enlargement of all sLNs, most *Zc3h12c-GFP<sup>KI / KI</sup>* mice presented with lymphadenopathy in only one or two sites. In contrast to the previous study, we observed that females were more likely to develop lymphadenopathy than males (Figure 2d). Following this observation, we used only females to characterize the phenotype. In addition, we observed that the proportion of *Zc3h12c-GFP<sup>KI / KI</sup>* mice with larger lymph nodes peaked between 3 and 6 months of age and decreased significantly in mice aged 12 months and older (data not shown). This observation suggests that the enlarged lymph nodes of *Zc3h12c-GFP<sup>KI / KI</sup>* mice atrophy with age, which is typical of the major physiological changes as part of aging.<sup>26</sup>

### The DC populations from the skin-draining lymph nodes express *Zc3h12c*

To further characterize and understand the expression pattern of *Zc3h12c*, we analyzed different cell populations in the spleen, lymph nodes (mucosal and skin-draining), bone marrow and skin (Figure 3, Supplementary figure 2) of our reporter mice by flow cytometry. In the sLN, the highest GFP expression was observed in the migratory conventional DC1 (cDC1) followed closely by the Langerhans cells (LCs) and the migratory cDC2.<sup>27</sup> A lower GFP signal was detected in the plasmacytoid DCs (pDCs), while resident cDC1 and cDC2 poorly expressed GFP. In the mesenteric lymph nodes, GFP expression in pDCs, cDC1 and cDC2 was markedly lower than that in the corresponding cells of the skin-draining nodes. In the

skin, low GFP expression was observed in the dermal mast cells, cDC1, cDC2 and T cells. Interestingly, while sLN LCs had the second highest levels of GFP expression, we could not detect any expression in skin LCs. In the spleen and bone marrow, pDCs expressed the highest levels of GFP. In general, B cells, T cells, macrophages, neutrophils and eosinophils expressed very low or undetectable levels of GFP, suggesting that *ZC3H12C* is poorly expressed in these populations. Thus, the results obtained from our GFP-reporter mouse strain essentially mirrored the expression profile of *Zc3h12c* mRNA that could be found in the *ImmGen* database and validated our new mouse model. Moreover, a comprehensive study of the DC transcriptional network identified *Zc3h12c* as part of the core cDC genes,<sup>28</sup> thus confirming the high expression of *Zc3h12c* in DCs.

### Enlarged *Zc3h12c*-deficient lymph nodes accumulate B cells and inflammatory DCs, but spleen develops normally

To better understand the causes of the lymph node hyperplasia in *Zc3h12c-GFP<sup>KI / KI</sup>* mice, we characterized the leukocyte populations in the enlarged lymph nodes and compared their proportions with those found in the lymph nodes from unaffected *Zc3h12c-GFP<sup>KI / KI</sup>* mice and from *Zc3h12c-GFP<sup>+ / +</sup>* mice. In accordance with the previously published observations, we found that the lymphadenopathy in *Zc3h12c-GFP<sup>KI / KI</sup>* mice was partly owing to a disorganized accumulation of B cells (Figure 4a).<sup>21</sup> However, we also observed a significant accumulation of myeloid cells, which had not been reported before, as shown with the large areas of CD11b<sup>+</sup> and F4/80<sup>+</sup> cells observed by immunostaining (Figure 4a). Similar to previous findings, we found that while wild-type and normal *Zc3h12c-GFP<sup>KI / KI</sup>* lymph nodes averaged a total of 3 million cells, enlarged lymph nodes averaged a total of 60 million cells, with some reaching up to 100 million cells (Figure 4b). We then analyzed B cells, T cells and DCs of *Zc3h12c-GFP<sup>KI / KI</sup>* mice with enlarged lymph nodes using flow cytometry and found a marked increase in their numbers (Figure 4c). We also observed a higher number of macrophages and monocytes (broadly defined as Ly6C<sup>+</sup>/MHCII<sup>+</sup> and MHCII<sup>+</sup>/Ly6C<sup>+</sup>, respectively; Figure 4c). In the enlarged LNs, we observed a population of Ly6C<sup>+</sup>/MHCII<sup>+</sup> cells that was absent from the wild-type and normal *Zc3h12c-GFP<sup>KI / KI</sup>* lymph nodes. We observed that this population expressed markers specific to inflammatory DCs, defined as CD11b<sup>+</sup>/Ly6C<sup>+</sup>/CD206<sup>+</sup>/FcεR1α<sup>+</sup>/CD64<sup>+</sup>/CD11c<sup>+</sup> (Figure 4d).<sup>29</sup> Therefore, we concluded that the accumulating myeloid cells in the enlarged lymph nodes of *Zc3h12c-GFP<sup>KI / KI</sup>* mice were a mix of inflammatory DCs, macrophages and monocytes.

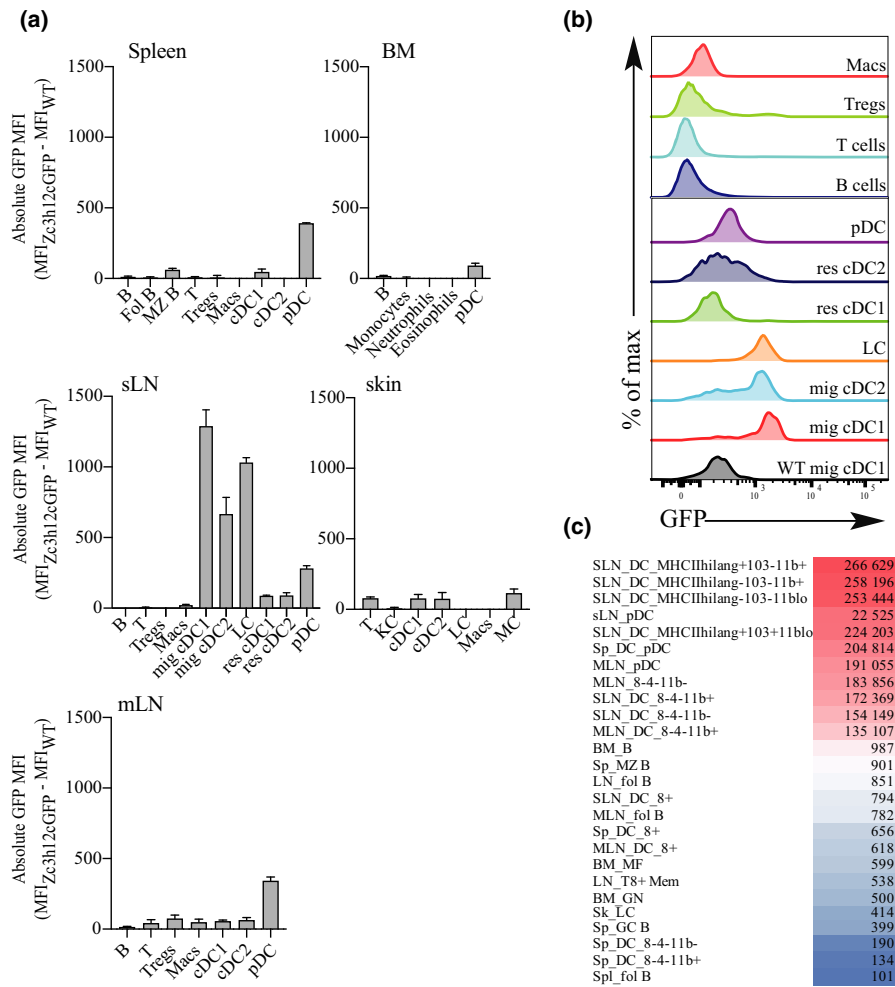


**Figure 3.** Characterization of the *Zc3h12c* messenger RNA (mRNA) expression pattern in immune cells and tissues. **(a)** Cells from different tissues of *Zc3h12c-GFP<sup>KI/KI</sup>* and *Zc3h12c-GFP<sup>+/+</sup>* animals were isolated as indicated. Green fluorescent protein (GFP) fluorescence was analyzed by flow cytometry, and cell-intrinsic autofluorescence observed in the cells from the *Zc3h12c-GFP<sup>+/+</sup>* mice was subtracted from the fluorescent signal from the cells from the *Zc3h12c-GFP<sup>KI/KI</sup>* mice. Results represent mean  $\pm$  s.d. of the difference between the s.e.m. of the *Zc3h12c-GFP<sup>+/+</sup>* group versus the *Zc3h12c-GFP<sup>KI/KI</sup>* group. Cells were gated as indicated in Supplementary figure 2. **(b)** Histogram showing the shift of GFP fluorescence observed in the indicated cell types in the skin-draining lymph nodes (sLNs). Cells were gated as indicated in Supplementary figure 2. **(c)** Heat map generated using *ImmGen* data and representing the levels of expression of *Zc3h12c* mRNA in indicated cell types. For the complete data set, refer to [http://rstats.immgen.org/Skyline\\_microarray/skyline.html](http://rstats.immgen.org/Skyline_microarray/skyline.html). BM, bone marrow; cDC, conventional dendritic cell; GFP, green fluorescent protein; LC, Langerhans cell; MFI, mean fluorescent intensity; mLN, mesenteric lymph node; MZ, marginal zone; pDC, plasmacytoid dendritic cell; Tregs, regulatory T cells; WT, wild type.

Given that lymphadenopathy was limited to the sLNs, we investigated whether this hyperplasia may result from changes in the skin. *Zc3h12c-GFP<sup>KI/KI</sup>* mice developing enlarged lymph nodes did not present any visible skin injury, redness, hair loss or scaling resembling skin inflammation or dermatitis. Histological analysis of skin samples from wild-type and *Zc3h12c-GFP<sup>KI/KI</sup>* mice did not appear different, even when samples were harvested close to an enlarged lymph node. No significant difference in epidermis and dermis thickness or in the proportion of immune cells was detected in *Zc3h12c-*

*GFP<sup>KI/KI</sup>* skin (Figure 4e). Flow cytometric analysis confirmed these results, as we did not find any major difference in leukocyte proportions between the skin drained by a normal lymph node and the skin drained by an enlarged lymph node (Figure 4f). Altogether, these results suggest that the lymphadenopathy observed is not a consequence of skin injury or inflammation. In keeping with the severe lymphadenopathy we observed, 18-week-old females had higher concentrations of TNF and of interferon- $\gamma$  in the serum (Figure 4g and von Gamm et al.<sup>21</sup>).

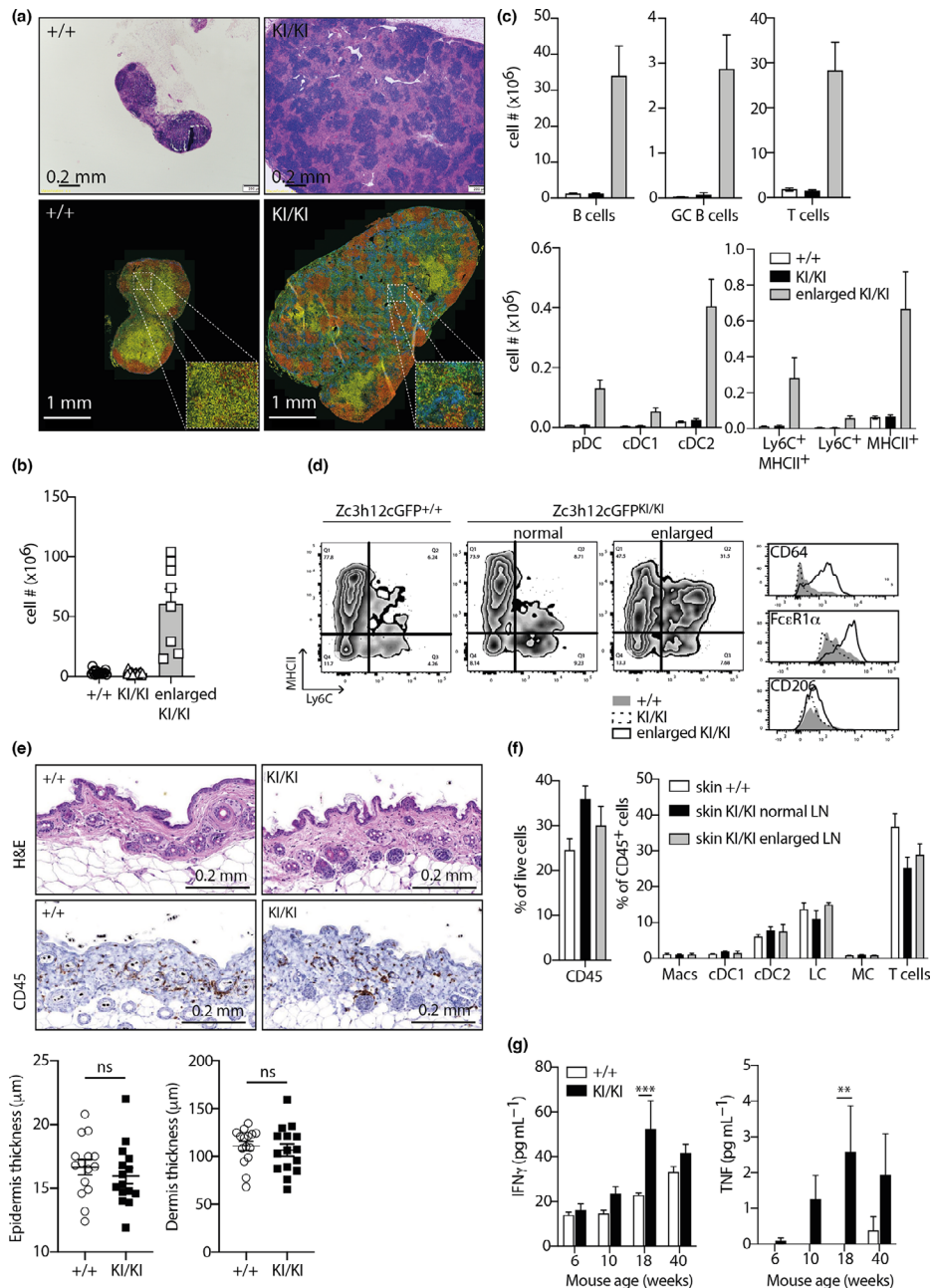


**Figure 4.** Phenotyping of *Zc3h12c-GFP<sup>KI/KI</sup>* mice. **(a)** Top panel: Lymph node sections from 200-day-old *Zc3h12c-GFP<sup>+/+</sup>* and *Zc3h12c-GFP<sup>KI/KI</sup>* mice, the latter exhibiting lymphadenopathy. Representative images. Scale bar = 0.2 mm. Bottom panel: Frozen lymph node sections were subjected to immunofluorescence staining for the analysis of B cells (anti-B220, in red), T cells (anti-CD3, in yellow) and myeloid cells (anti-F4/80 and anti-CD11b, in green and blue, respectively). Representative image. Scale bar = 1 mm. **(b)** Wild-type, normal (not enlarged) lymph nodes from *Zc3h12c-GFP<sup>KI/KI</sup>* mice and hypertrophic lymph nodes from *Zc3h12c-GFP<sup>KI/KI</sup>* mice were subjected to cell count and to **(c)** flow cytometric analysis of B cells, germinal center B cells (B220<sup>+</sup>GL7<sup>+</sup>), T cells, pDC, cDC1 and cDC2. **(d)** A population of Ly6C<sup>+</sup>MHCII<sup>+</sup> cells was observed uniquely in the hypertrophic lymph nodes from *Zc3h12c-GFP<sup>KI/KI</sup>* mice, expressing the markers CD64, FcεR1α and CD206. Results represent the mean ± s.e.m. of 18 animals per genotype, including eight *Zc3h12c-GFP<sup>KI/KI</sup>* mice with lymphadenopathy. **(e)** Histological analysis of the skin by routine hematoxylin and eosin (H&E) staining (top panel), immunohistochemistry (anti-CD45 staining, bottom panel). **(f)** Flow cytometric analysis of leukocytes from the skin from a wild-type mouse, skin surrounding a normal (non-enlarged) lymph node from a *Zc3h12c-GFP<sup>KI/KI</sup>* mouse and skin surrounding an enlarged lymph node from a *Zc3h12c-GFP<sup>KI/KI</sup>* mouse was performed. Results represent the mean ± s.e.m. of three animals per genotype. **(g)** Mice were subjected to mandible bleeds to collect serum at the indicated ages. Interferon-γ (IFNγ) and tumor necrosis factor (TNF) were detected in the serum by ELISA. Results represent the mean ± s.e.m. of eight animals per genotype. Statistical analysis was performed by two-way ANOVA. \*\**P* < 0.01; \*\*\**P* < 0.001. cDC, conventional dendritic cell; GC, germinal center; GFP, green fluorescent protein; KI, knock in; LN, lymph node; MHC, major histocompatibility complex; ns, not significant; pDC, plasmacytoid dendritic cell.

Spleens from *Zc3h12c-GFP<sup>KI/KI</sup>* mice appeared similar in size to the spleens of wild-type littermates. Previous observations suggested an impaired follicle development in *Regnase-3<sup>-/-</sup>* mice.<sup>21</sup> Using histological hematoxylin and eosin staining, we observed irregularly shaped follicles in the spleen of *Zc3h12c-GFP<sup>KI/KI</sup>* mice when compared with the spleen of *Zc3h12c-GFP<sup>+/+</sup>* littermates. To further investigate the follicle formation in these mice, we performed immunostaining of the spleen for macrophages (CD11b<sup>+</sup>), B cells (B220<sup>+</sup>) and metallophilic marginal zone macrophages (CD169<sup>+</sup>; Figure 3a). The latter, also known as MOMA1<sup>+</sup> metallophilic macrophages, typically form a ring-like structure around the lymphocyte follicles as they interact with marginal zone B cells. While the CD169<sup>+</sup> ring appeared thinner and more diffused in the spleen of *Zc3h12c-GFP<sup>KI/KI</sup>* mice than in the wild-type spleen (Supplementary figure 3a, b), we have not noted a convincing link between the loss of *Zc3h12c* and an impaired follicle formation. Proportions of T, B and DCs were identical in both genotypes, thus suggesting that the accumulation of B cells and inflammatory DCs was exclusive to sLN (Supplementary figure 3c). Spleen cellularity was similar to wild type in *Zc3h12c-GFP<sup>KI/KI</sup>* mice (Supplementary figure 3d). At last, cell populations in the mutant bone marrow of *Zc3h12c-GFP<sup>KI/KI</sup>* mice were normal, except for a slightly increased proportion of B cells (Supplementary figure 3e).

### Lymph node hyperplasia is driven by ablation of ZC3H12C in DCs

To determine whether the lymphadenopathy observed in homozygous animals is a result of the loss of *Zc3h12c* in the DCs, we crossed *Zc3h12c<sup>fl/fl</sup>* mice to *CD11c-cre<sup>T/+</sup>* animals. *CD11c-cre* mice achieve the deletion of the floxed allele of a gene of interest in the cDC1, cDC2, pDC and tissue-derived DC from lymph nodes, lung and skin.<sup>30</sup> We sorted splenic *CD11c<sup>+</sup>* cells and marginal zone B cells (as a control) and performed real-time-quantitative PCR with primers located in exons 2 and 3 to confirm the specific deletion of *Zc3h12c* in cells expressing *CD11c*. As expected, *CD11c<sup>+</sup>* cells deleted the floxed exon 2 efficiently, while *CD11c<sup>-</sup>* marginal B cells did not (Figure 5a). We observed that ablation of *Zc3h12c* in DCs (*CD11c-Zc3h12c<sup>fl/fl</sup> T/+*) resulted in the development of lymphadenopathy in mice aged between 4 and 7 months, similar to that observed in the germline knockout (*Zc3h12c-GFP<sup>KI/KI</sup>*), with disorganization of the B-cell follicles and accumulation of F4/80<sup>+</sup> and CD11b<sup>+</sup> myeloid cells (Figure 5b). Finally, about 70% of aging females and 11% of aging males developed the phenotype, similar to the proportions observed in the

*Zc3h12c-GFP<sup>KI/KI</sup>* mice (Figure 5c). We conclude that impairment of DC function is responsible for the lymphadenopathy associated with the loss of *Zc3h12c*.

### Loss of TNF prevents lymph node hyperplasia

Because of the regulatory effect of ZC3H12C on *Tnf* 3' UTR observed in our GFP reporter *in vitro* system, we hypothesized that DCs deficient in *Zc3h12c* would produce more TNF. We stimulated whole lymph node cells *ex vivo*, using lipopolysaccharide, CpG B, polyinosinic:polycytidylic acid (polyI:C) and IMQ and measured TNF production by DCs using flow cytometry (Figure 6a). Compared with control cells, we observed a trend toward a higher production of TNF in cDC2 from the lymph nodes of the *Zc3h12c-GFP<sup>KI/KI</sup>* mice, without treatment and following treatment with lipopolysaccharide, CpG B and IMQ (Figure 6b). We also observed an increase, yet not significant, of TNF production in the untreated pDCs from *Zc3h12c-GFP<sup>KI/KI</sup>* mice, and following treatment with lipopolysaccharide, CpG B and polyI:C.

Next, we hypothesized that *Zc3h12c-GFP<sup>KI/KI</sup>* mice would develop a TNF-dependent phenotype. Therefore, we crossed *Zc3h12c-GFP<sup>KI/KI</sup>* mice to *Tnf<sup>-/-</sup>* mice and analyzed the occurrence of lymph node hyperplasia in *Zc3h12c-GFP<sup>KI/KI</sup>/Tnf<sup>-/-</sup>* mice. Both males and females were analyzed and none of 52 double-mutant mice aged from 100 days to more than 2 years had developed enlarged lymph nodes in that period (Figure 6c). We thus conclude that loss of *Zc3h12c* impacts *Tnf* expression in DCs, which leads to lymphadenopathy in *Zc3h12c-GFP<sup>KI/KI</sup>* mice.

### Loss of *Zc3h12c* does not alter the development of imiquimod-induced psoriasis

*Zc3h12c* was previously identified as a risk factor for the development of psoriasis in two genome-wide association studies.<sup>22,31</sup> Although *Zc3h12c-GFP<sup>KI/KI</sup>* mice do not spontaneously develop psoriasis nor any other skin inflammation, even at an advanced age, we wanted to determine whether loss of ZC3H12C would influence the development of this illness. We thus used the IMQ-induced psoriasis-like skin inflammation model to investigate this question.<sup>32,33</sup> IMQ was applied daily on the skin at the back of *Zc3h12c-GFP<sup>+/+</sup>* and *Zc3h12c-GFP<sup>KI/KI</sup>* mice for 5–6 days. At the end of the treatment, we analyzed the skin for the hallmarks of psoriatic lesions (scaling and redness, thickening of the epidermis) by histology. A clear thickening of the epidermis (acanthosis) and scaling were observed after treatment, indicating the efficacy of IMQ in inducing psoriasis-like

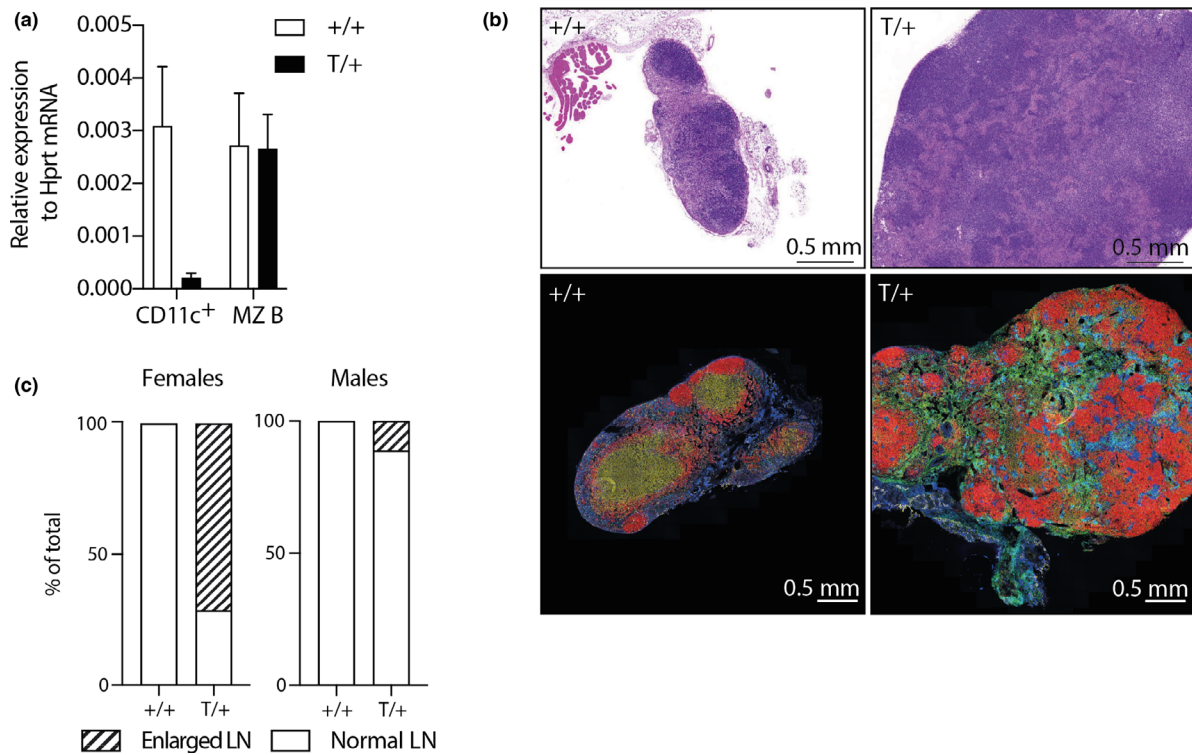


**Figure 5.** Dendritic cell (DC)-specific ablation of *Zc3h12c* causes lymphadenopathy. **(a)** Splenic CD11c<sup>+</sup> cells and marginal zone B cells were sorted, and their total RNA was extracted to assess the levels of expression of *Zc3h12c*. Results represent the mean  $\pm$  s.e.m. of four animals per genotype. **(b)** *Top panel:* Lymph node (LN) sections from 200-day-old *CD11c-Zc3h12c<sup>fl/fl</sup> +/+* (+/+) and *CD11c-Zc3h12c<sup>fl/fl</sup> T/+* (T/+) mice; the latter exhibiting lymphadenopathy. Representative images. Scale bar = 0.5 mm. *Bottom panel:* Frozen LN sections were subjected to immunofluorescence staining for the analysis of B cells (anti-B220, in red), T cells (anti-CD3, in yellow) and myeloid cells (anti-F4/80 and anti-CD11b, in green and blue, respectively). Representative image. Scale bar = 0.5 mm. **(c)** Proportion of lymphadenopathy (patterned area) observed in females and males in *CD11c-Zc3h12c<sup>fl/fl</sup> +/+* and *CD11c-Zc3h12c<sup>fl/fl</sup> T/+* mice. Data represent 44 *CD11c-Zc3h12c<sup>fl/fl</sup> +/+* and 49 *CD11c-Zc3h12c<sup>fl/fl</sup> T/+* animals, between 4 and 7 months of age. mRNA, messenger RNA.

skin inflammation. No major difference between *Zc3h12c-GFP<sup>KI/KI</sup>* and *Zc3h12c-GFP<sup>+/+</sup>* mice could be noted by histology (Figure 7a, b). To measure immune cell infiltration and the fluctuation of *Zc3h12c* expression induced by the treatment, we analyzed portions of IMQ-treated and untreated skin by flow cytometry and monitored the GFP signal in each cell type. Upon IMQ treatment, *Zc3h12c* was induced in dermal cDC1 and LC and reduced in dermal neutrophils. We also observed a significant increase of *Zc3h12c* expression in migratory cDC2 in the sLNs draining the IMQ-treated skin, suggesting that ZC3H12C has a role in the migratory program of dermal DCs (Supplementary figure 4a). As expected, we saw a large increase in the proportions of neutrophils and macrophages in the psoriatic skin, while the proportion of LC significantly dropped. We did not see any major change in the proportions of cDC1, cDC2 and total T cells. Overall, the dermal immune response to psoriasis development was similar across the two

cohorts (Supplementary figure 4b). We analyzed the sLN adjacent to the treated and untreated skin and observed an increased proportion of macrophages and neutrophils in the lymph nodes draining the treated skin, with no difference across both cohorts (Supplementary figure 4c).

We also assessed the production of proinflammatory cytokines during the treatment. While we could see an increase in TNF, IL-6 and interferon- $\gamma$  in the skin following treatment (Figure 7c) and an increase of TNF and IL-6 in the blood peaking 1 day after the first application (Figure 7d), we did not see a significant difference between the two genotypes. Finally, we analyzed the expression of critical cytokines and antimicrobial peptides in the skin and compared the expression levels between treated and untreated to measure the induction of the expression by the treatment (Figure 7e). Interestingly, we found higher induction of *S100a8* mRNA, which, together with



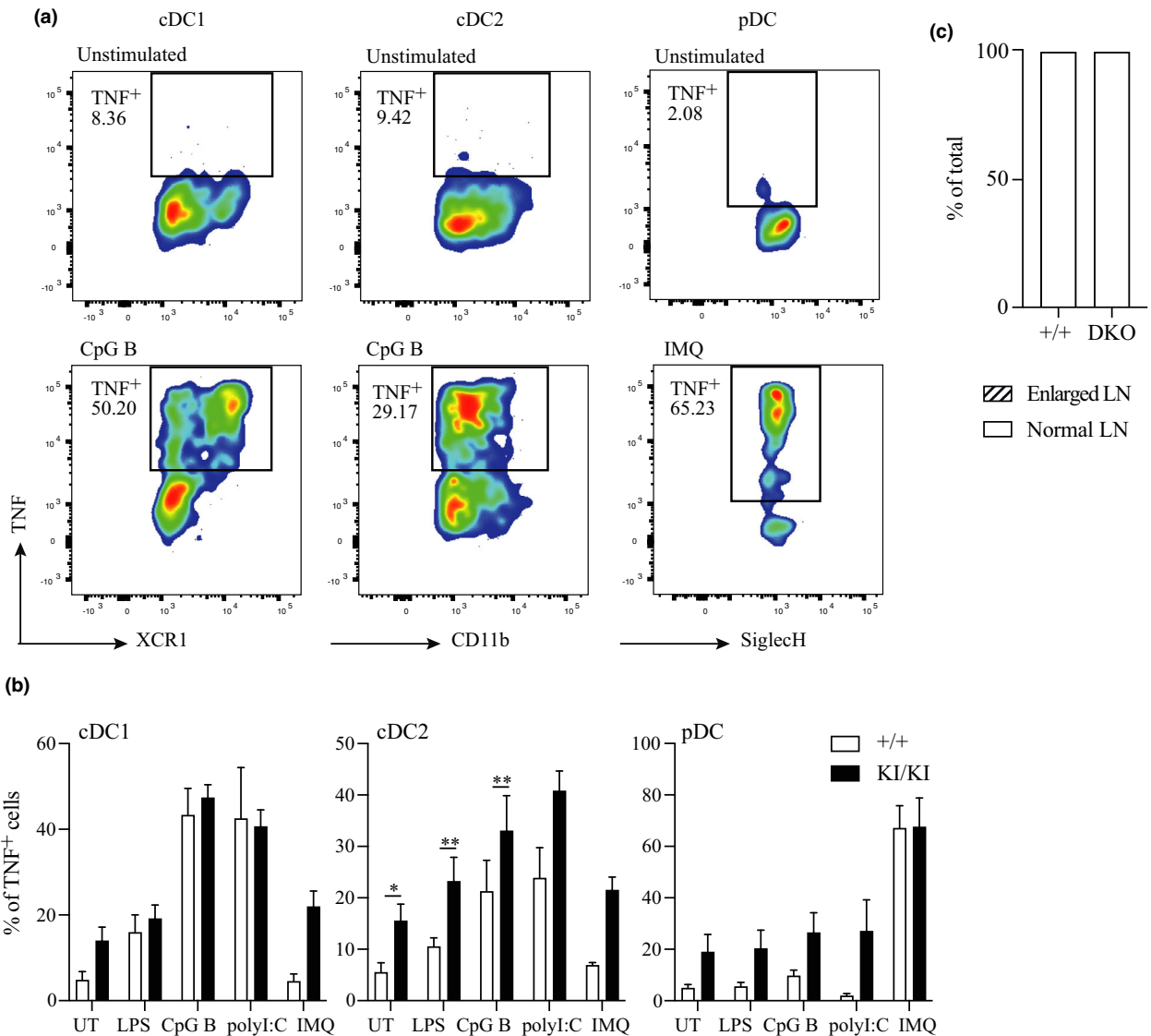


**Figure 6.** Tumor necrosis factor (TNF) is responsible for the development of lymphadenopathy. **(a)** Cells from lymph nodes of *Zc3h12c-GFP<sup>+/+</sup>* and *Zc3h12c-GFP<sup>KI/KI</sup>* mice were isolated and subsequently treated with the indicated TLR ligands [lipopolysaccharide (LPS) 50 ng mL<sup>-1</sup>; CpG B 1 μM; polyinosinic:polycytidylic acid (polyI:C) 10 μg mL<sup>-1</sup>; IMQ 5 μg mL<sup>-1</sup>] for 4 h together in the presence of Brefeldin A. Cells were first stained for surface markers (CD19, TCRb, CD11b, SiglecH, CD11c, MHCII, XCR1) and with a live/dead cell discriminating dye and intracellularly stained for TNF. **(b)** Cells were analyzed by flow cytometry and the percentages of TNF<sup>+</sup> cells were determined in the pDCs, cDC1 and cDC2 populations. Results represent the mean ± s.e.m. of 11 mice over three independent experiments. Statistical analysis was performed by two-way ANOVA; \**P* ≤ 0.05; \*\**P* < 0.01. **(c)** The proportion of lymphadenopathy (patterned area) observed in females and males in wild-type (*n* = 19) and *Zc3h12c-GFP<sup>KI/KI</sup>/Tnf<sup>-/-</sup>* (*n* = 52) mice, between 3 and 12 months of age. cDC, conventional dendritic cell; GFP, green fluorescent protein; IMQ, imiquimod; KI, knock-in; LN, lymph node; MHCII, major histocompatibility complex class II; pDC, plasmacytoid dendritic cell.

*S100a9*, plays a critical role in modulating the inflammatory response and leukocyte recruitment.<sup>34</sup> By contrast, *Zc3h12c-GFP<sup>KI/KI</sup>* mice showed reduced expression of the antimicrobial peptide *LL-37*. We did not detect any *Il-17* and *Il-19* in the treated skin (data not shown), and we did not see any difference in the expression of other key interleukins such as *Il-23a* and

*Il-22*, chemokines and chemokine receptors such as *Cxcr4*, *Ccr7* and *Cxcl12*. Altogether, we did not see any significant difference in the outcome of psoriasis development and in the associated immune response between wild-type and *Zc3h12c-GFP<sup>KI/KI</sup>* mice, suggesting that loss of *ZC3H12C* is dispensable for psoriasis development in this model.

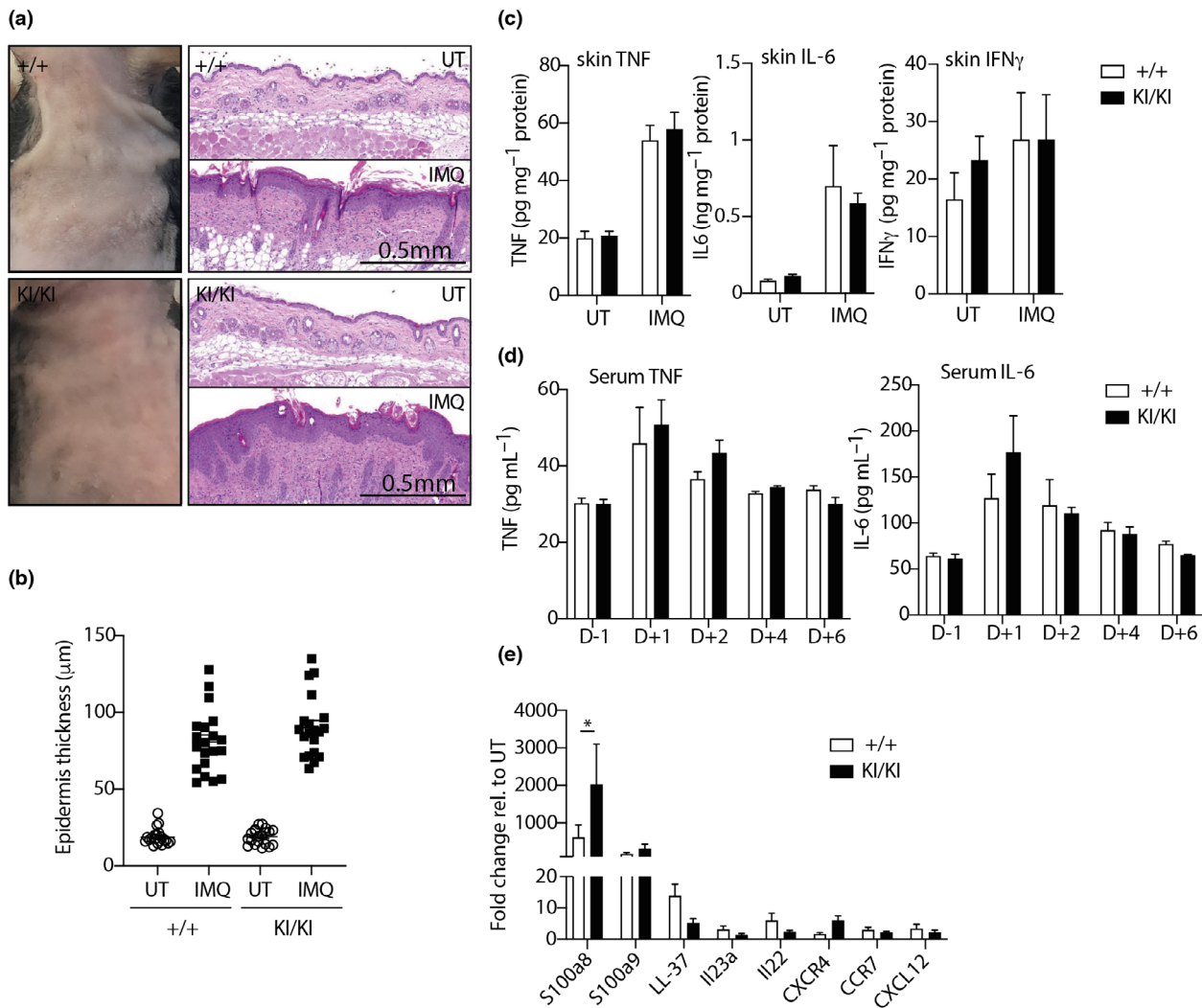


**Figure 7.** Characterization of the psoriasis-like skin inflammation in *Zc3h12c-GFP<sup>KI/KI</sup>* mice symptoms using the imiquimod (IMQ) model. **(a)** Representative photo of the skin of mice of the indicated genotypes following 5–6 days of topical IMQ application, and histological analysis of the untreated and IMQ-treated skin by routine hematoxylin and eosin staining. **(b)** Analysis of the epidermis thickness of untreated and IMQ-treated skin in *Zc3h12c-GFP<sup>+/+</sup>* and *Zc3h12c-GFP<sup>KI/KI</sup>* mice. **(c)** Levels of tumor necrosis factor (TNF), interleukin-6 (IL-6) and interferon- $\gamma$  (IFN $\gamma$ ) were measured in mice of the indicated genotypes in the skin after treatment and **(d)** TNF and IL-6 measured in the serum at different time points during the treatment. **(e)** Quantitative PCR analysis of the expression of messenger RNAs encoding key mediators of psoriasis in the skin from IMQ-treated and untreated mice of the indicated genotypes. Results represent the mean  $\pm$  s.e.m. of five animals per genotype and treatment and are representative of three independent experiments. Statistical analysis was performed by two-way ANOVA. \* $P \leq 0.05$ . cDC, conventional dendritic cell; GFP, green fluorescent protein; KI, knock-in; LN, lymph node; MHC, major histocompatibility complex; pDC, plasmacytoid dendritic cell.

## DISCUSSION

Over the years, studies have highlighted the importance of RBPs in regulating the levels of proinflammatory cytokines and other mediators of immune responses. More than 1500 RBPs have been identified with many involved in the control of immune responses. ZC3H12A, ZFP36 and Roquin remain the three most extensively studied RBPs involved in regulating the

levels of TNF<sup>8,35</sup> and other proinflammatory cytokines, such as IL-6.<sup>18</sup> The multiplicity of effects associated with RBPs are confounding and most likely reflects the insufficient knowledge we have of these proteins. Studies on binding specificities of ZC3H12 proteins are starting to emerge<sup>36,37</sup> and will help better define their functions.

In this study, we showed that while mice deficient in *Zc3h12c* developed normally and did not present with

any major abnormalities later in life, most individuals developed hyperplasia of sLNs as they aged. The extensive amino acid similarity between all four members of the ZC3H12 family of proteins and the proximity of their genes in the genome may indicate functional overlap and explain why lymphadenopathy develops in only about 70% of the *Zc3h12c*-deficient animals. Although a previous study also observed lymphadenopathy in *Zc3h12c*-deficient mice, we are the first to report the prevalence of female mice developing the phenotype and the accumulation of inflammatory DCs in the enlarged lymph nodes. In line with the expression profile from *ImmGen*, we demonstrated that ZC3H12C is highly expressed in DC populations and particularly in migratory cDC2s and LCs, but not in tissue macrophages and bone marrow-derived macrophages as reported (Supplementary figure 5, von Gamm *et al.*<sup>21</sup>). One reason for this discrepancy is that the LysM-Cre transgene was used in the previous study to delete *Zc3h12c* from the myeloid compartment which, in addition to macrophages, also targets about half of the DCs, particularly the monocyte-derived DCs.<sup>38</sup> We also confirmed the role of DCs in the development of lymphadenopathy by specifically deleting *Zc3h12c* expression from the DC populations.

We reveal here that ZC3H12C is involved in regulating *Tnf* expression *in vitro* by destabilizing *Tnf* 3' UTR mRNA via its RNase activity, which is conserved across all members of the ZC3H12 subfamily. *Zc3h12c-GFP<sup>K1/K1</sup>* mice also produced more TNF than their wild-type counterparts, and the absence of *Tnf* prevented the development of lymphadenopathy in *Zc3h12c-GFP<sup>K1/K1</sup>* mice, thus suggesting that *Zc3h12c* plays a role in regulating *Tnf* expression both *in vitro* and *in vivo*.

The high expression of *Zc3h12c* in DCs in the sLNs and the identification of *Zc3h12c* as a risk gene for the development of psoriasis in humans suggested that ZC3H12C plays a role in skin homeostasis. We have investigated the predicted association of *Zc3h12c* with the development of psoriasis in humans by using the IMQ-induced psoriasis-like skin inflammation but only saw a mild impact of the loss of *Zc3h12c* in this model. While this model is most widely used for preclinical psoriasis studies, because of its convenience and induction of psoriasis-like histological features, the compound's mechanism of action is poorly understood.<sup>32</sup> In human psoriasis, keratinocytes play a primary role in inducing an immune response following physical trauma or bacterial infection, leading to a cascade of events involving DCs and T cells, ultimately causing excessive keratinocyte proliferation and epidermis thickening. However, in the IMQ model, keratinocytes are not the primary cells activated by the

TLR ligand as they lack expression of TLR7/8. Therefore, the difference in the mechanisms of induction could account for the absence of differences in psoriasis development in mice lacking *Zc3h12c* versus humans with polymorphisms in ZC3H12C. Importantly, we observed an induction of *Zc3h12c* expression in migratory cDC2s in the sLN and in the LCs in the skin following IMQ treatment, suggesting that *Zc3h12c* plays a role in the migratory program of these DCs. Finally, the exact mechanism by which hyperplasia of sLN develops remains to be investigated, particularly the processes that drive the accumulation of inflammatory DCs in the pathologically enlarged lymph nodes, which are typically observed following monocyte recruitment induced by parasitic infections, viral infections and immunization.<sup>29</sup>

## METHODS

### Generation of the *Zc3h12c-GFP* and *Zc3h12c-flox* mice

The MAGEC laboratory (WEHI) generated the strains using previously published protocols (Kueh *et al.*<sup>39</sup>). Briefly, DNA constructs were assembled *in vitro* to place the different elements (GFP or loxP sites) in their desired positions. These constructs were injected together with a single guide RNA (targeting a PAM site inside exon 2 of *Zc3h12c*) and recombinant Cas9 protein into fertilized one-cell-stage embryos to promote DNA repair and homologous recombination. Animals were screened for these events by PCR and recombinant alleles were sequenced to confirm adequate modifications.

### Reporter mice

GFP fluorescence in different *Zc3h12c-GFP<sup>K1/K1</sup>* cell types was analyzed using a flow cytometer and compared with the mean fluorescence intensity of the corresponding cells of their *Zc3h12c-GFP<sup>+/+</sup>* counterparts. Because wild-type and knock-out cells are independent populations that cannot be randomly paired, we calculated the average of the GFP mean fluorescence intensity for each cell type across both genotypes. We then subtracted this averaged GFP mean fluorescent intensity of wild-type cells, which corresponded to the autofluorescence of the cells, from the averaged GFP mean fluorescent intensity of *Zc3h12c-GFP<sup>K1/K1</sup>* cells, which represents the actual GFP signal. Any negative value obtained following this subtraction was systematically set to 0.

### *Tnf* 3' UTR reporter assays

GFP reporter constructs engineered as in Lacey *et al.*<sup>11</sup> contained an SV40 early promoter driving the expression of enhanced GFP. Murine *Tnf* 3' UTRs (wild type, BPSM1 mutant-derived or containing deletions of regions 1–6 as

indicated)<sup>12</sup> were inserted between the *XbaI* and *BamHI* sites. HEK293 cells were transiently transfected using FuGENE 6 (Promega, Madison, WI, USA) with GFP-*Tnf* 3' UTR reporter constructs and a pGL3-mCherry control construct and analyzed 3 days later by flow cytometry on an LSR IIW (BD Biosciences, Franklin Lane, NJ, USA). GFP mean fluorescence intensity was calculated on live mCherry-positive cells and compared with that of empty vector control-transduced cells.

### Bone marrow-derived DCs

Bone marrow-derived DCs (BMDCs) were extracted from the femur and tibiae of mice and cultured for at least 7 days in Roswell Park Memorial Institute medium supplemented with 10% heat-inactivated fetal calf serum, 50  $\mu$ M  $\beta$ -mercaptoethanol (Sigma, St Louis, MO, USA), 1 $\times$  GlutaMAX (Gibco, Thermo Fisher Scientific, Waltham, MA), 100 ng mL<sup>-1</sup> Flt3-L (BioXcell, Lebanon, NH, USA) at 37°C, 10% CO<sub>2</sub> at 1.5  $\times$  10<sup>6</sup> cells mL<sup>-1</sup>. The day before treatment, cells were detached using Trypsin-ethylenediaminetetraacetic acid (Sigma) and replated as needed for the assay.

### Bone marrow-derived macrophages

Bone marrow-derived macrophages were generated from the femora and tibiae of mice and cultured for 7 days in DMEM supplemented with 10% heat-inactivated fetal calf serum, 20% L929-conditioned medium and penicillin/streptomycin at 37°C and 10% CO<sub>2</sub>. The day prior treatment, cells were detached using 5 mM ethylenediaminetetraacetic acid/phosphate-buffered saline and replated as needed for the assay.

### Antibodies

The list and characteristics of the antibodies used in this study are shown in Supplementary table 1.

### Flow cytometry

Mice were killed, their entire torso shaved and the residual fur removed with Nair hair removal cream. The subcutaneous fat was removed by gently scraping with a scalpel blade. Skin samples were then finely diced using scissors and transferred into a 50-mL Falcon tube with 2.5 mL of Liberase TM (Sigma; 0.1 mg mL<sup>-1</sup>) + DNase I (Sigma; 0.3 mg mL<sup>-1</sup>) in Roswell Park Memorial Institute medium. Samples were incubated at 37°C with agitation for a minimum of 90 min. After incubation, enzymes were inactivated using fluorescence-activated cell sorting (FACS) buffer (0.1% bovine serum albumin/5 mM ethylenediaminetetraacetic acid/phosphate-buffered saline), and suspensions were filtered through a 40- $\mu$ m cell strainer. Cells were spun down and resuspended in FACS buffer for further staining.

Lymph nodes and spleens were finely cut using scissors, and transferred into a tube with 1 or 2 mL of digestion mix made of collagenase IV (Gibco) and DNase I (0.3 mg mL<sup>-1</sup>) in Hanks' Balanced Salt Solution (Gibco; supplemented with

3 mM CaCl<sub>2</sub>). Samples were incubated at 37°C for 30 min under agitation. Enzymes were then inactivated using FACS buffer, and samples were filtered through a 70- or 40- $\mu$ m cell strainer (lymph node and spleen, respectively). Cells were then spun down and resuspended in 500 (lymph nodes) or 8 mL (whole spleen) of FACS buffer. For skin samples, cells were incubated with only Fc block (anti-CD16/CD32 monoclonal antibody; WEHI) for 30 min before staining. Cells were then stained with VD506 viability dye (Thermo Fisher Scientific, Waltham, MA, USA) for 10 min at 4°C in the dark, spun down and rinsed off. Next, cells were stained using the appropriate antibody staining mix in FACS buffer in a V-bottomed 96-well plate for 30 min at 4°C in the dark. For analysis of intracellular TNF, cells were stimulated with the indicated stimulant plus 1 $\times$  Brefeldin A (BD Bioscience, Franklin Lane, NJ, USA) for 4 h. Cells were then stained for any relevant surface markers and fixed for 20 min at 4°C in the dark (Cytofix/Cytoperm; BD Biosciences). Finally, cells were stained for intracellular TNF using an anti-TNF antibody (CST). Cells were then analyzed using a Fortessa X1, X20 or Symphony analyzer, and data were analyzed and calculated with FlowJo software (version 10).

### Histology and immunostaining

For routine histology, tissues were fixed in 10% formalin for 24 h and then transferred into 70% ethanol before paraffin embedding and sectioning. All slides were scanned on a 3DHISTECH Panoramic Scan II scanner (Leica Biosystems Nussloch GmbH) and analyzed with CaseViewer 2.2.1 for Mac.

For immunostaining and frozen section histology, tissues were fixed in 4% paraformaldehyde for 24 h, and cryoprotected in 30% sucrose/ddH<sub>2</sub>O until they sank. Tissues were then embedded in optimal cutting temperature compound freezing media (Sakura Finetek), frozen using a PrestoCHILL (Milestone Medical, Kalamazoo, MI, USA) and stored at -80°C until further use. Then, 8- $\mu$ m sections were cut using a Cryostat Microtome HM550 (Leica Biosystems Nussloch GmbH) and adhered on Superfrost Plus (ESBE Scientific, Markham, ON, Canada) slides. Slides were dried at room temperature for at least 30 min, and then stored at -20°C until use. Slides were rinsed with TBS + 0.5% Tween20, and contours were drawn using a hydrophobic pen. Slides were blocked using goat normal serum or fetal calf serum (5% in TBS + 0.3% Triton X-100) for 30 min. Slides were incubated overnight at 4°C with the appropriate primary antibodies, washed three times for 5 min each and incubated with streptavidin conjugated to A594 for 1 h at room temperature. After three washing steps, slides were mounted using the Fluoroshield mounting medium (Sigma) and imaged using a 780 or 880 Zeiss confocal microscope, and data were analyzed using ImageJ software.

### Imiquimod-induced psoriasis-like skin inflammation model

Cohorts of at least four mice were shaved 1 day before the treatment, under an isoflurane inhalant anesthetic. Then,

62.5 mg of Aldara cream (3M, St Paul, MN, USA) was applied onto the shaved skin at the same time for 5–6 consecutive days using a sterile cotton tip. Mice were collected 24 h after the last topical application. Once killed, a patch of untreated skin was shaved, and both treated and untreated skin were depilated using Nair or Veet hair removal cream. After 2 min, the hair removal cream was thoroughly rinsed off using cold water. Treated and untreated skin samples were cut into four sections, for flow cytometric, RNA, protein and histology analysis.

### Sample preparation for ELISA and quantitative PCR

Whole skin samples (~100 µg) were lysed in ice-cold DISC lysis buffer [20 mM Tris pH 7.5, 2 mM ethylenediaminetetraacetic acid, 1% Triton X-100, 150 mM NaCl, 10% glycerol, complete cocktail protease inhibitor (Sigma) in H<sub>2</sub>O] using a TissueLyser (Qiagen; Venlo, Limburg, Netherlands) at 28 Hz for 3 × 1 min and left on ice for 60 min. Samples were then spun at 13 000 rpm for 15 min, and the supernatants were collected for protein analysis (ELISA). Supernatants were diluted 1/10 for protein quantification using a bicinchoninic acid kit (Thermo Fisher Scientific). TNF, interferon- $\gamma$  and IL-6 ELISAs were performed using eBioscience kits (Thermo Fisher Scientific), and the IL-1 $\beta$  ELISA was performed using the R&D Systems kit, following the manufacturers' recommendations. Data presented are calculated as pg or ng of cytokine mg<sup>-1</sup> of total protein.

For RNA extraction, whole skin samples were homogenized in TRIzol (Qiagen; Venlo, Limburg, Netherlands) using a TissueLyser (Qiagen) at 28 Hz for 3 × 1 min and processed according to the manufacturer's recommendations. The concentration of total RNA in a solution was measured using a NanoDrop (Thermo Fisher Scientific); 2 µg of total RNA was used as template for cDNA synthesis using oligo(dT) with the Tetro cDNA synthesis kit (Bioline, Meridian Bioscience, London, Ontario) according to the manufacturer's protocol. Freshly synthesized cDNA was diluted one-third and 1 µL of the diluted cDNA was used for real-time-PCR, using the SensiFAST SYBR Hi-ROX Kit (Bioline), and run on a QuantStudio 12K. Differential gene expression was calculated using the  $\Delta$ Ct method.

### ACKNOWLEDGMENTS

We thank J Stanley, J Martin, L Spencer and G Siciliano for animal care and expertise; A Tsai and E Carr for animal genotyping. This work was supported by the Australian NHMRC (Program Grant 461221, Research Fellowship 1042629, Project grant 1127885), the Arthritis Australia Zimmer fellowship and infrastructure support from the NHMRC (IRISS) and the Victorian State Government (OIS). Generation of *Zc3h12c*-GFP and *Zc3h12c*-flox mice used in this study was supported by the Australian Phenomics Network (APN) and the Australian Government through the National Collaborative Research Infrastructure Strategy (NCRIS) program.

### CONFLICT OF INTEREST

The authors declare no conflict of interest.

### AUTHOR CONTRIBUTIONS

**Philippe Bouillet:** Conceptualization; Funding acquisition; Methodology; Project administration; Resources; Supervision; Writing—review & editing. **Elise Clayer:** Formal analysis; Investigation; Methodology; Resources; Writing—original draft. **Daniel Frank:** Investigation; Resources. **Holly Anderton:** Investigation; Resources. **Shengbo Zhang:** Investigation. **Andrew Kueh:** Investigation; Resources. **Valentin Heim:** Investigation. **Stephen L Nutt:** Validation; Writing—review & editing. **Michael Chopin:** Formal analysis; Supervision; Writing—review & editing.

### DATA AVAILABILITY STATEMENT

The data and materials, including animals, that support the findings of this study are available on request from the corresponding author.

### REFERENCES

- Brennan FM, Feldmann M. Cytokines in autoimmunity. *Curr Opin Immunol* 1996; **8**: 872–877.
- Drutskaya MS, Efimov GA, Astrakhantseva IV, Kruglov AA, Nedospasov SA. Making anti-cytokine therapy more selective: studies in mice. *Cytokine* 2018; **101**: 33–38.
- Ettehadi P, Greaves MW, Wallach D, Aderka D, Camp RD. Elevated tumour necrosis factor- $\alpha$  (TNF- $\alpha$ ) biological activity in psoriatic skin lesions. *Clin Exp Immunol* 1994; **96**: 146–151.
- Papadakis KA, Targan SR. Role of cytokines in the pathogenesis of inflammatory bowel disease. *Annu Rev Med* 2000; **51**: 289–298.
- Tetta C, Camussi G, Modena V, Di Vittorio C, Baglioni C. Tumour necrosis factor in serum and synovial fluid of patients with active and severe rheumatoid arthritis. *Ann Rheum Dis* 1990; **49**: 665–667.
- Radner H, Aletaha D. Anti-TNF in rheumatoid arthritis: an overview. *Wien Med Wochenschr* 2015; **165**: 3–9.
- Han J, Brown T, Beutler B. Endotoxin-responsive sequences control cachectin/tumor necrosis factor biosynthesis at the translational level. *J Exp Med* 1990; **171**: 465–475.
- Taylor GA, Carballo E, Lee DM, *et al.* A pathogenetic role for TNF $\alpha$  in the syndrome of cachexia, arthritis, and autoimmunity resulting from tristetraprolin (TTP) deficiency. *Immunity* 1996; **4**: 445–454.
- Kontoyiannis D, Pasparakis M, Pizarro TT, Cominelli F, Kollias G. Impaired on/off regulation of TNF biosynthesis in mice lacking TNF AU-rich elements: implications for joint and gut-associated immunopathologies. *Immunity* 1999; **10**: 387–398.

10. Leppik K, Schott J, Reitter S, Poetz F, Hammond MC, Stoecklin G. Roquin promotes constitutive mRNA decay via a conserved class of stem-loop recognition motifs. *Cell* 2013; **153**: 869–881.
11. Lacey D, Hickey P, Arhatari BD, *et al.* Spontaneous retrotransposon insertion into TNF 3'UTR causes heart valve disease and chronic polyarthritis. *Proc Natl Acad Sci USA* 2015; **112**: 9698–9703.
12. Clayer E, Dalseno D, Kueh A, *et al.* Severe impairment of TNF post-transcriptional Regulation leads to embryonic death. *iScience* 2020; **23**: 101726.
13. Gerstberger S, Hafner M, Tuschl T. A census of human RNA-binding proteins. *Nat Rev Genet* 2014; **15**: 829–845.
14. Otsuka H, Fukao A, Funakami Y, Duncan KE, Fujiwara T. Emerging evidence of translational control by AU-rich element-binding proteins. *Front Genet* 2019; **10**: 332.
15. Fu M, Blackshear PJ. RNA-binding proteins in immune regulation: a focus on CCCH zinc finger proteins. *Nat Rev Immunol* 2017; **17**: 130–143.
16. Andrienne M, Assabban A, La C, *et al.* Tristetraprolin expression by keratinocytes controls local and systemic inflammation. *JCI Insight* 2017; **2**: e92979.
17. Bertesi M, Fantini S, Alecci C, *et al.* Promoter methylation leads to decreased ZFP36 expression and deregulated nlrp3 inflammasome activation in psoriatic fibroblasts. *Front Med (Lausanne)* 2020; **7**: 579383.
18. Matsushita K, Takeuchi O, Standley DM, *et al.* Zc3h12a is an RNase essential for controlling immune responses by regulating mRNA decay. *Nature* 2009; **458**: 1185–1190.
19. Maeda K, Akira S. Regulation of mRNA stability by CCCH-type zinc-finger proteins in immune cells. *Int Immunol* 2017; **29**: 149–155.
20. Liang J, Wang J, Azfer A, *et al.* A novel CCCH-zinc finger protein family regulates proinflammatory activation of macrophages. *J Biol Chem* 2008; **283**: 6337–6346.
21. von Gamm M, Schaub A, Jones AN, *et al.* Immune homeostasis and regulation of the interferon pathway require myeloid-derived Regnase-3. *J Exp Med* 2019; **216**: 1700–1723.
22. Tsoi LC, Spain SL, Knight J, *et al.* Identification of 15 new psoriasis susceptibility loci highlights the role of innate immunity. *Nat Genet* 2012; **44**: 1341–1348.
23. Lai WS, Carballo E, Strum JR, Kennington EA, Phillips RS, Blackshear PJ. Evidence that tristetraprolin binds to AU-rich elements and promotes the deadenylation and destabilization of tumor necrosis factor alpha mRNA. *Mol Cell Biol* 1999; **19**: 4311–4323.
24. Xu J, Peng W, Sun Y, *et al.* Structural study of MCP1P1 N-terminal conserved domain reveals a PIN-like RNase. *Nucleic Acids Res* 2012; **40**: 6957–6965.
25. Yokogawa M, Tsushima T, Noda NN, *et al.* Structural basis for the regulation of enzymatic activity of Regnase-1 by domain-domain interactions. *Sci Rep* 2016; **6**: 22324.
26. Turner VM, Mabbott NA. Influence of ageing on the microarchitecture of the spleen and lymph nodes. *Biogerontology* 2017; **18**: 723–738.
27. Kashem SW, Haniffa M, Kaplan DH. Antigen-presenting cells in the skin. *Annu Rev Immunol* 2017; **35**: 469–499.
28. Miller JC, Brown BD, Shay T, *et al.* Deciphering the transcriptional network of the dendritic cell lineage. *Nat Immunol* 2012; **13**: 888–899.
29. Segura E, Amigorena S. Inflammatory dendritic cells in mice and humans. *Trends Immunol* 2013; **34**: 440–445.
30. Caton ML, Smith-Raska MR, Reizis B. Notch-RBP-J signaling controls the homeostasis of CD8<sup>+</sup> dendritic cells in the spleen. *J Exp Med* 2007; **204**: 1653–1664.
31. Munir S, Rahman SB, Rehman S, *et al.* Association analysis of GWAS and candidate gene loci in a Pakistani population with psoriasis. *Mol Immunol* 2015; **64**: 190–194.
32. Hawkes JE, Gudjonsson JE, Ward NL. The snowballing literature on imiquimod-induced skin inflammation in mice: a critical appraisal. *J Invest Dermatol* 2017; **137**: 546–549.
33. van der Fits L, Mourits S, Voerman JS, *et al.* Imiquimod-induced psoriasis-like skin inflammation in mice is mediated via the IL-23/IL-17 axis. *J Immunol* 2009; **182**: 5836–5845.
34. Wang S, Song R, Wang Z, Jing Z, Wang S, Ma J. S100A8/A9 in Inflammation. *Front Immunol* 2018; **9**: 1298.
35. Stoecklin G, Lu M, Rattenbacher B, Moroni C. A constitutive decay element promotes tumor necrosis factor alpha mRNA degradation via an AU-rich element-independent pathway. *Mol Cell Biol* 2003; **23**: 3506–3515.
36. Jolma A, Zhang J, Mondragon E, *et al.* Binding specificities of human RNA-binding proteins toward structured and linear RNA sequences. *Genome Res* 2020; **30**: 962–973.
37. Garg A, Roske Y, Yamada S, Uehata T, Takeuchi O, Heinemann U. PIN and CCCH Zn-finger domains coordinate RNA targeting in ZC3H12 family endoribonucleases. *Nucleic Acids Res* 2021; **49**: 5369–5381.
38. McCubbrey AL, Allison KC, Lee-Sherick AB, Jakubczik CV, Janssen WJ. Promoter specificity and efficacy in conditional and inducible transgenic targeting of lung macrophages. *Front Immunol* 2017; **8**: 1618.
39. Kueh AJ, Pal M, Tai L, *et al.* An update on using CRISPR/Cas9 in the one-cell stage mouse embryo for generating complex mutant alleles. *Cell Death Differ* 2017; **24**: 1821–1822.

## SUPPORTING INFORMATION

Additional supporting information may be found online in the Supporting Information section at the end of the article.

© 2022 The Authors. *Immunology & Cell Biology* published by John Wiley & Sons Australia, Ltd on behalf of Australian and New Zealand Society for Immunology, Inc.

This is an open access article under the terms of the Creative Commons Attribution-NonCommercial-NoDerivs License, which permits use and distribution in any medium, provided the original work is properly cited, the use is non-commercial and no modifications or adaptations are made.